

Włodzimierz Andrzej BEDNAREK\*  
Poznań University of Technology  
Institute of Civil Engineering

**THE INFLUENCE OF BALLAST LONGITUDINAL  
RESISTANCE ON AXIAL DISPLACEMENT STATE IN  
CWR TRACK DUE TO LOCAL RAIL  
TEMPERATURE CHANGES**

*Received: 18 March 2008*

*Accepted: 12 December 2008*

In the paper several specified models of ballast longitudinal resistance to behaviour of CWR track have been analysed. The considered problem is connected with local track segments in which horizontal displacements of rail cross-sections occur. The displacements occur mainly because of real non-uniform temperature distributions over the length of CWR track (e.g. variable insolation of rail, variable temperature of rails to sleepers fastening) [11,12,16]. On the grounds of empirical characteristics, the obtained formulae and dependences allowed an analysis of displacement distribution along the track and also an examination of forces and stress distribution. Similar phenomenon also occurs within the so-called 'breathing' ends of CWR track [5,9]. A significant influence of railway works (e.g. railway tamping) on a range of local temperature changes interaction along the track has been shown [1,2].

Key words: CWR track; ballast longitudinal resistance; rail axial displacement; local rail temperature changes

## 1. INTRODUCTION

Horizontal displacements of track  $u$  due to temperature changes generate a horizontal reaction of ballast -  $r(u)$ , which depends on its rail displacement  $u$

---

\* Corresponding author. Tel.: -; fax: -.

E-mail address: [wlodzimierz.bednarek@put.poznan.pl](mailto:wlodzimierz.bednarek@put.poznan.pl) (W.A. Bednarek)

of cross-section of a track (Fig. 1) [3,13,15]. The resultant reaction, acting at a certain eccentricity relative to the rail axis, causes track bending in a vertical plane [2,3,14,15].

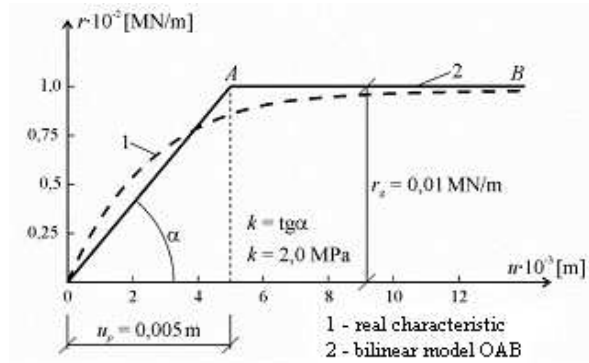


Fig. 1. Characteristics of ballast longitudinal resistance  $r(u)$

A longitudinal resistance of the ballast in the track depends above all on: the kind and condition of rail fastening to the sleepers, type and spacing of the sleepers, kind, quantity and degree of the ballast consolidation. The resistance can also be influenced by temperature, humidity and ballast pollution as well as track maintenance.

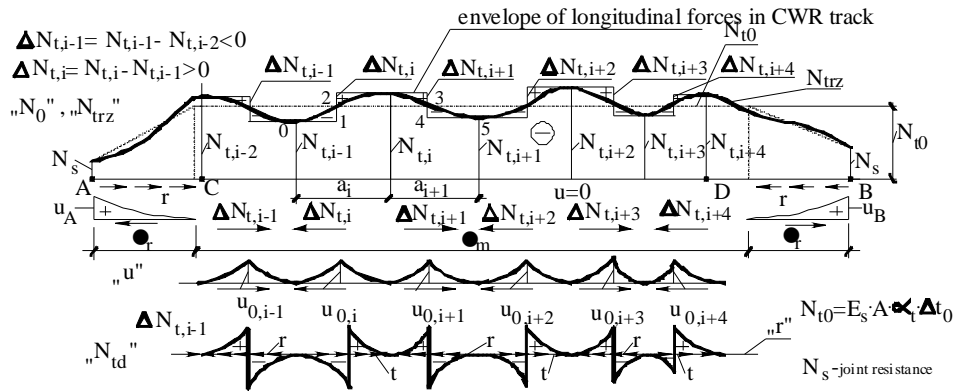
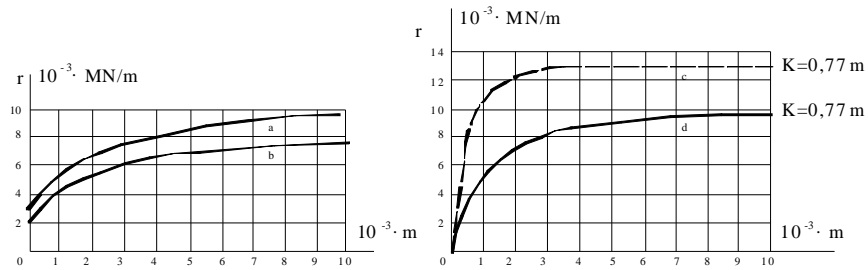


Fig. 2. Schematic analytical drawings

As can be seen in the diagram, ballast resistance  $r(u)$  depends (in a non-linear way) on thermal displacement  $u$  of the track till certain displacement limit

is reached. Above this point, it assumes the limit value of  $r_g$  and does not change despite a further increase in displacement  $u$  (Fig. 1).

a)



b)

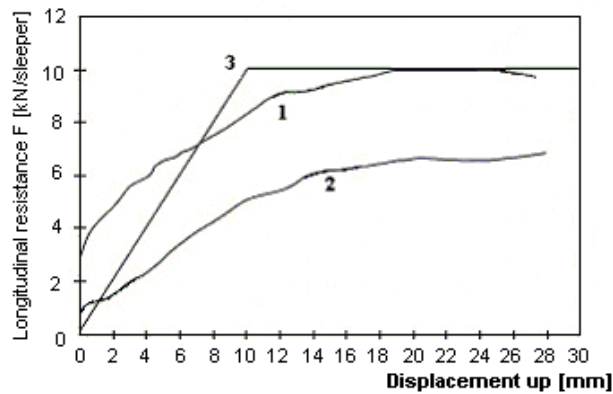


Fig. 3. Ballast longitudinal resistance [8]

- a) a – longitudinal resistance at wooden sleeper spacing of 65 cm (22 sleepers per span)
- b – longitudinal resistance at wooden sleeper spacing of 65 cm (11 sleepers per span)
- c – longitudinal resistance at variable wooden sleeper spacing (K- sleeper spacing)
- d – longitudinal resistance at variable pre-stressed concrete sleeper spacing (K- spacing)
- b) wooden sleepers: 1 – consolidated ballast; 2 – tamped ballast; 3 – supplementary model

Considering the effect of horizontal CWR track displacements occurring locally, due to non-uniform rail temperature distribution  $t$ , one should take into account the variable ballast resistance over the track length and variable thermal conditions, occurring during track laying. They are generally characterized by a variable temperature of the rail to sleeper fixing  $t_p$ . The temperature difference occurring while fixing in track cross-sections  $\Delta t = t - t_p$ , causes a non uniform distribution of longitudinal thermal force  $N_t = E_s \cdot A \cdot \alpha_t \cdot \Delta t$  [11] in the real

continuous welded rail track. Its course is shown schematically by the continuous line in Fig. 2. This non-uniformity is additionally increased by the influence of continuous welded rail track creep under traffic, which causes unfavourable changes in the temperature layout  $t_p$  [3]. A dashed line in Fig. 2 denotes, on the other hand, the analytical distribution of thermal force  $N_{t0}$ . For the distribution of  $N_{t0}$  in the central part of  $CD$  ( $N_{t0} = const.$ ) we have  $u=0$  (confined length of CWR track). On the other hand  $u \neq 0$  (2<sup>nd</sup> order parabola) occurs over the - so called - moving (breathing) ends of length  $l_r$ , where  $N_{t0}$  is of linear distribution (for  $r = r_g$ , Fig. 4a). The computed (trapezoidal) distribution of  $N_{t0}$  in Fig. 2 thus corresponds to the case of the behaviour of a straight, CWR track at a uniform temperature increase over its entire length, for  $t_p = const.$  [2,3].

## 2. CHARACTERISTICS OF BALLAST LONGITUDINAL RESISTANCE IN THE RAILWAY TRACK

The characteristics of longitudinal track resistance obtained empirically on the basis of the influence of railway works (e.g. railway tamping) are shown in Fig. 3 [4,8].

In order to simplify the track stability problem, the real, non-linear characteristic of longitudinal resistance is most often replaced by linear models (F

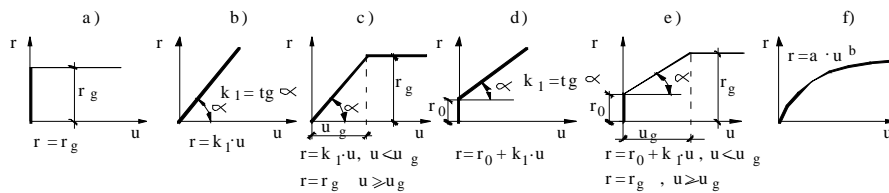


Fig. 4. Models of longitudinal resistance of the ballast

## 3. LONGITUDINAL DISPLACEMENT STATE IN CWR TRACK DUE TO LOCAL RAIL TEMPERATURE CHANGES

Arising forces  $\Delta N$  over the length of the track, due to local temperature differences (shown schematically in Fig. 2), cause local, zoned horizontal

displacements of transverse rail cross-sections, of maximum values from  $u_{0,i-1}$  to  $u_{0,i+4}$ . The longitudinal track displacements in turn induce the horizontal reaction of ballast  $r(u)$  to the degree allowed by the value of  $u$ . For the description of function  $r(u)$  several models shown in Fig. 4 have been used.

Considering e.g. the influence of force

$$\Delta N_{ti} = N_{t,i} - N_{t,i-1} = E_S \cdot A \cdot \alpha_t \cdot (\Delta t_i - \Delta t_{i-1})$$

on the behaviour of the track, assuming  $r = r_g$  (model from Fig. 4a), we obtain [2,3,10]

$$u = \frac{r_g}{2 \cdot E_S \cdot A} \cdot x^2 - \frac{\Delta N_{ti}}{2 \cdot E_S \cdot A} \cdot x + \frac{\Delta N_{ti}^2}{8 \cdot E_S \cdot A \cdot r_g}, \quad (3.1)$$

$$N_{td} = r_g \cdot x - \frac{\Delta N_{ti}}{2}, \quad l_w = \frac{\Delta N_{ti}}{2 \cdot r_g}. \quad (3.2)$$

The calculation schematics and the approximate course of  $u$  and  $N_{td}$  functions in local co-ordinates are shown in Figs. 5 and 6.

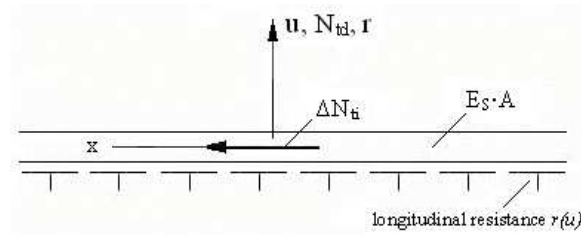


Fig. 5. Calculation sketch

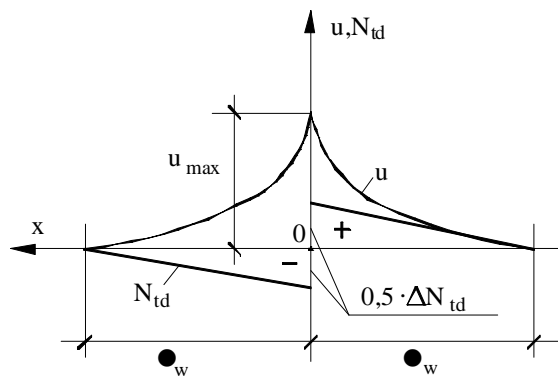


Fig. 6. Diagrams of functions  $u$  and  $N_{td}$

For the model from Fig. 4b, with  $r = k_1 \cdot u$ , we obtain [2,6]:

$$u = \frac{\Delta N_{ti}}{2 \cdot E_S \cdot A \cdot \sqrt{\alpha}} \cdot e^{-\sqrt{\alpha} \cdot x}, \quad N_{td} = -\frac{\Delta N_{ti}}{2} \cdot e^{-\sqrt{\alpha} \cdot x}, \quad l_w = \infty \quad (3.3)$$

where  $\alpha = \frac{k_1}{E_S \cdot A}$  (basic railway parameter in the longitudinal direction [6]).

In turn, for the model from Fig. 4d, with  $r = r_0 + k_1 \cdot u$ , we obtain

$$u = -\frac{\beta}{\alpha} \cdot \left[ 1 - \cosh\left(\sqrt{\alpha} \cdot x\right) \mp \operatorname{arcsinh}\left(\frac{\Delta N_{ti} \cdot \sqrt{\alpha}}{2 \cdot \beta \cdot E_S \cdot A}\right) \right], \quad (3.4)$$

$$N_{td} = \frac{\beta \cdot E_S \cdot A}{\sqrt{\alpha}} \cdot \left[ \sinh\left(\sqrt{\alpha} \cdot x\right) \mp \operatorname{arcsinh}\left(\frac{\Delta N_{ti} \cdot \sqrt{\alpha}}{2 \cdot \beta \cdot E_S \cdot A}\right) \right], \quad (3.5)$$

$$l_w = \frac{1}{\sqrt{\alpha}} \cdot \operatorname{arcsinh}\left(\frac{\Delta N_{ti} \cdot \sqrt{\alpha}}{2 \cdot \beta \cdot E_S \cdot A}\right), \quad (3.6)$$

where  $\alpha = \frac{k_1}{E_S \cdot A}$ ,  $\beta = \frac{r_0}{E_S \cdot A}$  (basic railway parameters in the longitudinal direction [6]).

If  $u_{\max} > u_g$ , one should apply a model of roadbed e.g. from Fig. 4e. For this model of roadbed longitudinal resistance, we obtain [2]:

for  $0 \leq x \leq a_1$ ,

$$u = \frac{\gamma}{2} \cdot (x^2 - a_1^2) - \left( \gamma \cdot a_1 + \frac{\beta^*}{\sqrt{\alpha}} \cdot \sinh(\sqrt{\alpha} \cdot a_2) \right) \cdot (x - a_1) + u_g, \quad (3.7)$$

$$a_1 = \frac{1}{\gamma} \cdot \left( \alpha_t \cdot \bar{\Delta}t - \frac{\beta^*}{\sqrt{\alpha}} \sinh(\operatorname{arccosh}(\delta)) \right), \quad (\text{linear distribution of } \Delta N), \quad (3.8)$$

for  $a_1 \leq x \leq a_r$ ,

$$u = -\frac{\beta^*}{\alpha} \cdot \left( 1 - \cosh(\sqrt{\alpha} \cdot (a_r - x)) \right), \quad (3.9)$$

$$a_2 = \frac{1}{\sqrt{\alpha}} \arccos h(\delta), \text{ (non-linear distribution of } \Delta N), \quad (3.10)$$

$$a_r = a_1 + a_2, \quad (3.11)$$

where:

$$\delta = 1 + \frac{\alpha}{\beta^*} \cdot u_g, \quad \alpha = \frac{k_1}{E_S \cdot A}, \quad \beta^* = \frac{r_0}{E_S \cdot A},$$

$$\gamma = \frac{r_g}{E_S \cdot A} = \frac{r_0 + k_1 \cdot u}{E_S \cdot A} = \beta^* + \alpha \cdot u_g, \quad \alpha_t \cdot \overline{\Delta t} = \frac{\sigma_t}{E_S} = \frac{\Delta N_{ti}}{2 \cdot E_S \cdot A}.$$

### 3.1. Examples of computations

The computations were carried out for CWR track UIC60 (60E1) (wooden sleepers, crushed stone ballast), assuming the local co-ordinates (Fig. 5) and taking the following data into account:

$$E_S \cdot A = 3228 \text{ MN}, \quad \alpha_t = 1.15 \cdot 10^{-5} \frac{1}{\text{K}}, \quad r_0 = 0.003 \text{ MN/m},$$

$$r_g = 0.010 \text{ MN/m}, \quad k_1 = 1.4 \text{ MPa}, \quad u_g = 0.005 \text{ m} \text{ (c.f. Figs. 1 and 3a).}$$

$$\text{We assumed: } \Delta(\Delta t)_i = 7.0 \text{ K}, \text{ where: } \Delta(\Delta t)_i = \frac{\Delta N_{ti}}{E_S \cdot A \cdot \alpha_t}, \text{ at which}$$

$$\Delta N_{ti} = N_{ti} - N_{t,i-1} = E_S \cdot A \cdot \alpha_t \cdot (\Delta t_i - \Delta t_{i-1}),$$

$\Delta t_i = t_i - t_{pi} - t_s$ ,  $\Delta t_{i-1} = t_{i-1} - t_{p,i-1} - t_s$ ,  $t$  - rail temperature,  $t_p$  - temperature at rail fastening to the sleepers,  $t_s = \frac{N_s}{E_S \cdot A \cdot \alpha_t}$ ,  $N_s$  - horizontal reaction at the rail joint due to thermal effects, ( $N_s \cong 0.20 \text{ MN}$ ),

$$\Delta(\Delta t)_i = \Delta t_i - \Delta t_{i-1} = (t_i - t_{i-1}) - (t_{pi} - t_{p,i-1}).$$

$$\text{Hence } \Delta N_{ti} = E_S \cdot A \cdot \alpha_t \cdot \Delta(\Delta t)_i = 0.26 \text{ MN}.$$

For the above data we obtain:

1° - model from Fig. 4a.

$$u = 1.549 \cdot 10^{-6} \cdot x^2 \mp 4.027 \cdot 10^{-5} \cdot x + 2.618 \cdot 10^{-4},$$

for:  $x > 0, (-), x < 0, (+)$ .

For  $x = 0$ ,  $u_{\max} = 2.618 \cdot 10^{-4}$  m, i.e.  $u_{\max} < u_g = 5.0 \cdot 10^{-3}$  m.

$N_{td} = 0.01 \cdot x \mp 0.130$ ,  $x > 0, (-), x < 0, (+)$ ,  $l_w = 13.0$  m,

$r = r_g = -E_S \cdot A \cdot \frac{d^2 u}{dx^2} = -0.01$  MN/m (in accordance with the assumed model).

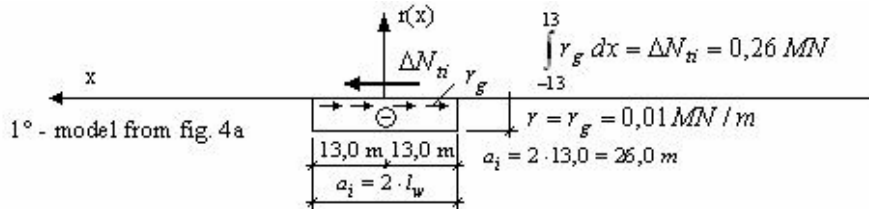


Fig. 7. Distribution of function  $r(x)$  for the model from Fig. 4a

2° - model from Fig. 4b.

$$\alpha = \frac{k_1}{E_S \cdot A} = 4.3369 \cdot 10^{-4} \text{ m}^{-2}, \quad \sqrt{\alpha} = 2.0826 \cdot 10^{-2} \text{ m}^{-1},$$

$u = 1.9338 \cdot 10^{-3} \cdot \exp(\mp 2.0826 \cdot 10^{-2} \cdot x)$ , for  $x > 0, (-), x < 0, (+)$ .

For  $x = 0$ ,  $u_{\max} = 1.9338 \cdot 10^{-3}$  m, i.e.  $u_{\max} < u_g = 5.0 \cdot 10^{-3}$  m.

$$r = -E_S \cdot A \cdot \frac{d^2 u}{dx^2} = -k_1 \cdot u = -2.7073 \cdot 10^{-3} \cdot \exp(\mp 2.0826 \cdot 10^{-2} \cdot x),$$

for  $x = 0$ ,  $r_{\min} = -2.7073 \cdot 10^{-3}$  MN/m,

$$N_{td} = E_S \cdot A \cdot \frac{du}{dx} = \mp 0.130 \cdot \exp(\mp 2.0826 \cdot 10^{-2} \cdot x),$$

$l_w = \infty$ ,  $\lim_{x \rightarrow \pm\infty} N_{td} = 0$ ,  $\lim_{x \rightarrow \pm\infty} r = 0$  (in accordance with the assumed model).

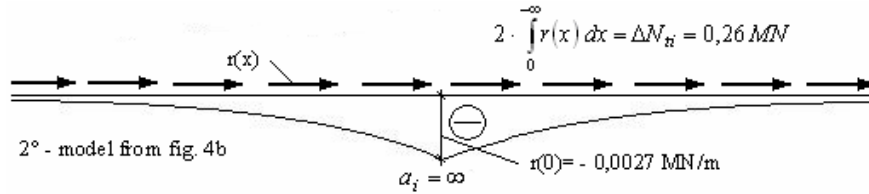


Fig. 8. Distribution of function  $r(x)$  for the model from Fig. 4b

3° - model from Fig. 4d.

$$\alpha = 4.3369 \cdot 10^{-4} \text{ m}^{-2}, \quad \beta = \frac{l_0}{E_S \cdot A} = 9.2933 \cdot 10^{-7} \text{ m}^{-1},$$

$$u = -2.1429 \cdot 10^{-3} \cdot \left[ 1 - \cosh\left(2.0826 \cdot 10^{-2} \cdot x \mp \operatorname{arcsinh}(0.9024)\right) \right],$$

for:  $x > 0, (-), x < 0, (+)$ .

$$u = -2.1429 \cdot 10^{-3} \cdot \left[ 1 - \cosh\left(2.0826 \cdot 10^{-2} \cdot x \mp 0.8107\right) \right].$$

$$\text{For } x = 0, \quad u_{\max} = -2.1429 \cdot 10^{-3} \cdot (1 - 1.347) = 7.4354 \cdot 10^{-4} \text{ m},$$

$$\text{i.e. } \underline{u_{\max} < u_g = 5.0 \cdot 10^{-3} \text{ m}}.$$

$$N_{td} = E_S \cdot A \cdot \frac{du}{dx} = 0.1441 \cdot \sinh\left(2.0826 \cdot 10^{-2} \cdot x \mp 0.8107\right),$$

$$\text{for } x = 0, \quad N_{td} = \mp 0.13 \text{ MN}, \quad l_w = 38.9273 \text{ m}; \quad \text{for } x = l_w: \quad u = 0, \quad N_{td} = 0,$$

$$r = -E_S \cdot A \cdot \frac{d^2u}{dx^2} = -0.003 \cdot \cosh\left(2.0826 \cdot 10^{-2} \cdot x \mp 0.8107\right),$$

$$\text{for } x = \pm l_w, \quad r = -0.003 \text{ MN/m};$$

$$\text{for } x = 0, \quad r = -1.347 \cdot 0.003 = -0.004041 \text{ MN/m}.$$

$$\omega = \int_0^{-l_w} r \, dx = 0,130 \text{ MN}, \quad r_{sr} = -\frac{\omega}{l_w} = -0.00334 \text{ MN/m}.$$

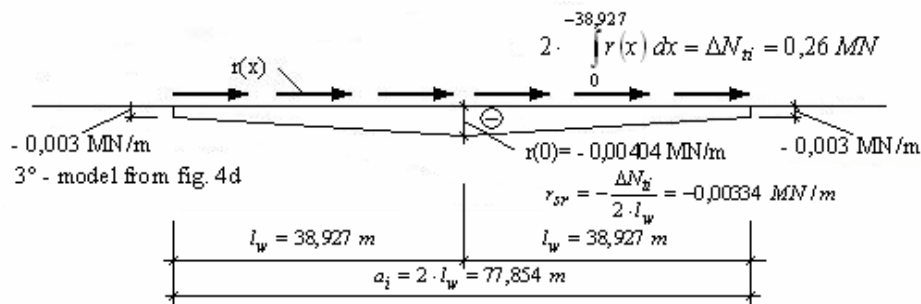


Fig. 9. Distribution of function  $r(x)$  for the model from Fig. 4d

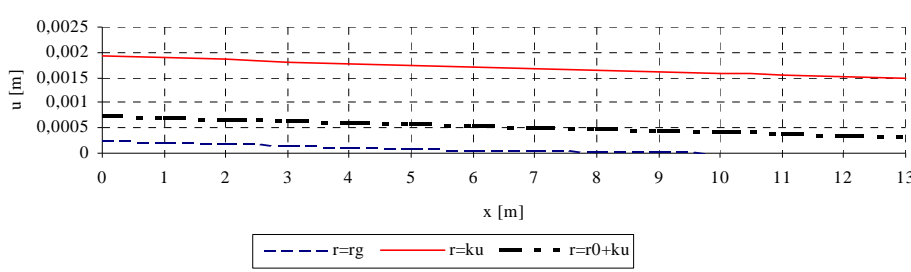


Fig. 10. Railway track axial displacements for different models

As can be seen, extreme displacements were obtained for model  $r(u) = k_1 \cdot u$ , and the smallest displacements for model  $r(u) = r_g$ .

For the data from Fig. 3 ( $r_0$ ,  $u_g$  and  $k_1$  in particular) we obtain:

#### - consolidated ballast

4° - the model from Fig. 4d

$$\alpha = 3.6430 \cdot 10^{-4} \text{ m}^{-2}, \quad \sqrt{\alpha} = 1.9087 \cdot 10^{-2} \text{ m}^{-1},$$

$$\beta = \frac{r_0}{E_S \cdot A} = 1.5613 \cdot 10^{-6} \text{ m}^{-1},$$

$$u = -4.2857 \cdot 10^{-3} \cdot \left[ 1 - \cosh\left(1.9087 \cdot 10^{-2} \cdot x \mp \operatorname{arcsinh}(0.4923)\right) \right],$$

for:  $x > 0, (-)$ ,  $x < 0, (+)$ .

$$u = -4.2857 \cdot 10^{-3} \cdot \left[ 1 - \cosh\left(1.9087 \cdot 10^{-2} \cdot x \mp 0.4743\right) \right].$$

For  $x = 0$ ,  $u_{\max} = -4.2857 \cdot 10^{-3} \cdot (1 - 1.1146) = 4.9122 \cdot 10^{-4} \text{ m}$ ,

i.e.  $u_{\max} < u_g = 1.0 \cdot 10^{-2} \text{ m}$ .

$$N_{td} = E_S \cdot A \cdot \frac{du}{dx} = 0.2641 \cdot \sinh\left(1.9087 \cdot 10^{-2} \cdot x \mp 0.4743\right),$$

for  $x = 0$ ,  $N_{td} = \mp 0.13 \text{ MN}$ ,  $l_w = 24.8513 \text{ m}$ ; for  $x = l_w$ :  $u = 0$ ,

$$N_{td} = 0,$$

$$r = -E_S \cdot A \cdot \frac{d^2u}{dx^2} = -0.00504 \cdot \cosh\left(1.9087 \cdot 10^{-2} \cdot x \mp 0.4743\right),$$

for  $x = \pm l_w$ ,  $r = -0.00504 \text{ MN/m}$ ;

for  $x = 0$ ,  $r = -1.1146 \cdot 0.00504 = -0.0056177 \text{ MN/m}$ .

$$\omega = \int_0^{-l_w} r dx = 0.130 \text{ MN}, r_{sr} = -\frac{\omega}{l_w} = -0.0052311 \text{ MN/m}.$$

5° - the model from Fig. 4b

$$\alpha = \frac{k_1}{E_S \cdot A} = 5.2043 \cdot 10^{-4} \text{ m}^{-2}, \sqrt{\alpha} = 2.2813 \cdot 10^{-2} \text{ m}^{-1},$$

$$u = 1.7653 \cdot 10^{-3} \cdot \exp(\mp 2.2813 \cdot 10^{-2} \cdot x), \text{ for } x > 0, (-), x < 0, (+).$$

$$\text{For } x = 0, u_{\max} = 1.7653 \cdot 10^{-3} \text{ m, i.e. } \underline{u_{\max} < u_g = 1.0 \cdot 10^{-2} \text{ m}}.$$

$$r = -E_S \cdot A \cdot \frac{d^2 u}{dx^2} = -k_1 \cdot u = -2.9657 \cdot 10^{-3} \cdot \exp(\mp 2.2813 \cdot 10^{-2} \cdot x),$$

$$\text{for } x = 0, r_{\min} = -2.9657 \cdot 10^{-3} \text{ MN/m},$$

$$N_{td} = E_S \cdot A \cdot \frac{du}{dx} = \mp 0.130 \cdot \exp(\mp 2.2813 \cdot 10^{-2} \cdot x),$$

$$l_w = \infty, \lim_{x \rightarrow \pm\infty} N_{td} = 0, \lim_{x \rightarrow \pm\infty} r = 0 \text{ (in accordance with the assumed model)}.$$

- **tamped ballast** (Fig. 3)

6° - the model from Fig. 4d

$$\alpha = 2.6021 \cdot 10^{-4} \text{ m}^{-2},$$

$$\sqrt{\alpha} = 1.6131 \cdot 10^{-2} \text{ m}^{-1}, \beta = \frac{r_0}{E_S \cdot A} = 5.2043 \cdot 10^{-7} \text{ m}^{-1},$$

$$u = -2.0 \cdot 10^{-3} \cdot [1 - \cosh(1.6131 \cdot 10^{-2} \cdot x \mp 1.0465)],$$

$$\text{for: } x > 0, (-), x < 0, (+).$$

$$\text{For } x = 0, u_{\max} = 1.1988 \cdot 10^{-3} \text{ m, i.e. } \underline{u_{\max} < u_g = 1.0 \cdot 10^{-2} \text{ m}}.$$

For the tamped ballast, contrasted to the consolidated ballast, we have:

$$\frac{1.1988 \cdot 10^{-3}}{4.9122 \cdot 10^{-4}} = 2.44, \text{ i.e. about 2.5-times increase in the displacement}$$

for  $x = 0$ .

$$N_{td} = E_S \cdot A \cdot \frac{du}{dx} = 0.1041 \cdot \sinh(1.6131 \cdot 10^{-2} \cdot x \mp 1.0465),$$

$$\text{for } x = 0, N_{td} = \mp 0.13 \text{ MN},$$

$l_w = 64.8742$  m (i.e. 2.61-times greater  $l_w$  than for the consolidated ballast);

for  $x = l_w$  we have:  $u = 0$ ,  $N_{td} = 0$ ,

$$r = -E_S \cdot A \cdot \frac{d^2 u}{dx^2} = -0.00168 \cdot \cosh(1.6131 \cdot 10^{-2} \cdot x \mp 1.0465),$$

for  $x = \pm l_w$ ,  $r = -0.00168$  MN/m; for  $x = 0$ ,  
 $r = -0.002687$  MN/m.

$$\omega = \int_0^{-l_w} r dx = 0.130 \text{ MN}, \quad r_{sr} = -\frac{\omega}{l_w} = -0.0020039 \text{ MN/m}.$$

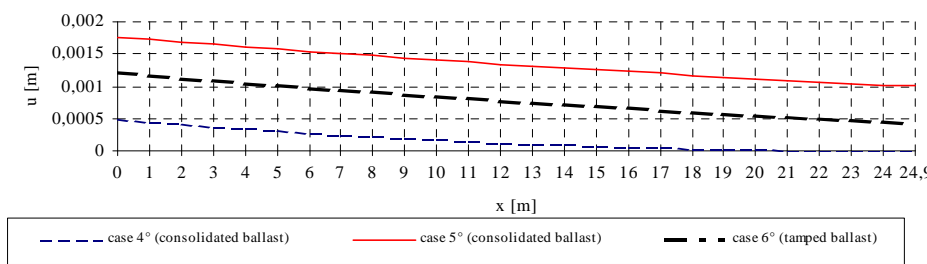


Fig. 11. Railway track axial displacement for different ballast state

The diagram above shows the influence of both the ballast consolidation and the model assumed on the analysis of rail longitudinal displacements. In the case of greater temperature differences along the track reaching a value of  $20 \div 23$  [K] [7], we obtain:  $u > u_g$ . For this case the model from Fig. 4e is suitable.

Considering only the right part of the railway track for which we have  $\frac{\Delta N}{2}$  we obtain:

**- consolidated ballast (Fig. 3)**

7° - the model from Fig. 4e

Value of  $\Delta t = 23$  [K] was assumed (from condition:  $a_1 = 0$ , we have:

$$\Delta t = \beta^* \cdot \sqrt{(\delta - 1)} \cdot \frac{\sqrt{(\delta + 1)}}{\alpha_t \cdot \sqrt{\alpha}}, \text{ resulting in: } \Delta t = 22.62 \text{ [K]} \text{ giving:}$$

$$\alpha = 3.6430 \cdot 10^{-4} \text{ m}^{-2}, \quad \beta^* = 1.5613 \cdot 10^{-6} \text{ m}^{-1}, \quad \delta = 3,333,$$

$$\gamma = 5.2043 \cdot 10^{-6} \text{ m}^{-1}, \alpha_t \cdot \overline{\Delta t} = 2.6450 \cdot 10^{-4};$$

$$a_1 = 0.8442 \text{ m}, a_2 = 98.1746 \text{ m} \rightarrow a_r = 99.0188 \text{ m},$$

<p style="text-align: center;">for <math>0 \leq x \leq a_1</math>:</p> $u(0) = 1.0221 \cdot 10^{-2} \text{ m},$ $u(a_1) = 1.0 \cdot 10^{-2} \text{ m},$ $r(0) = 0.0168 \frac{\text{MN}}{\text{m}},$ $r(a_1) = 0.0168 \frac{\text{MN}}{\text{m}},$	<p style="text-align: center;">for <math>a_1 \leq x \leq a_r</math>:</p> $u(a_1) = 1.0 \cdot 10^{-2} \text{ m},$ $u(a_r) = 0.0 \text{ m},$ $r(a_1) = 0.0168 \frac{\text{MN}}{\text{m}},$ $r(a_r) = 0.00504 \frac{\text{MN}}{\text{m}}.$
---	---

**- tamped ballast (Fig. 3)**

8° - the model from Fig. 4e

Value of  $\Delta t = 17 \text{ [K]}$  was assumed (from condition:  $a_1 = 0$ , we have:

$$\Delta t = \beta^* \cdot \sqrt{(\delta - 1)} \cdot \frac{\sqrt{(\delta + 1)}}{\alpha_t \cdot \sqrt{\alpha}}, \text{ resulting in: } \Delta t = 16.59 \text{ [K]} \text{ giving:}$$

$$\alpha = 2.6021 \cdot 10^{-4} \text{ m}^{-2}, \beta^* = 5.2043 \cdot 10^{-7} \text{ m}^{-1}, \delta = 6.0,$$

$$\gamma = 3.1226 \cdot 10^{-6} \text{ m}^{-1}, \alpha_t \cdot \overline{\Delta t} = 1.9550 \cdot 10^{-4};$$

$$a_1 = 1.4840 \text{ m}, a_2 = 153.6091 \text{ m} \rightarrow a_r = 155.0931 \text{ m},$$

<p style="text-align: center;">for <math>0 \leq x \leq a_1</math>:</p> $u(0) = 1.0287 \cdot 10^{-2} \text{ m},$ $u(a_1) = 1.0 \cdot 10^{-2} \text{ m},$ $r(0) = 0.01008 \frac{\text{MN}}{\text{m}},$ $r(a_1) = 0.01008 \frac{\text{MN}}{\text{m}},$	<p style="text-align: center;">for <math>a_1 \leq x \leq a_r</math>:</p> $u(a_1) = 1.0 \cdot 10^{-2} \text{ m},$ $u(a_r) = 0.0 \text{ m},$ $r(a_1) = 0.01008 \frac{\text{MN}}{\text{m}},$ $r(a_r) = 0.00168 \frac{\text{MN}}{\text{m}}.$
---	--

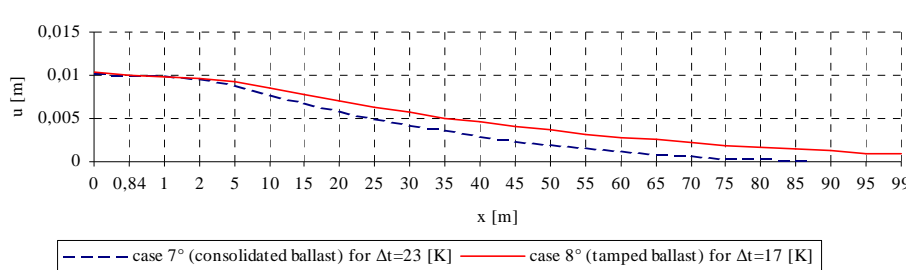


Fig. 12. Railway track axial displacement for consolidated and tamped ballasts

As can be seen, in spite of smaller temperature difference, displacements for the tamped ballast have greater values and a greater action range (for  $u > u_g$  model 4e).

#### 4. CONCLUSIONS

1. In the paper the influence of railway works (e.g. railway tamping) on action range of  $\Delta N$  force on distribution of displacements  $u(x)$  and resistance  $r(u)$  along the track has been shown.
2. From the above analysis the influence of the actual ballast state on the longitudinal displacement can be determined. For the consolidated ballast (Fig. 3) the critical temperature increase for model  $e$  amounts to 23 [K] (case 7°), and for the tamped ballast (case 8°) 17 [K]. The action range of the increased thermal force also increases from 99.02 m for the consolidated ballast to 155.09 m for the tamped ballast.
3. For small temperature increases ( $\Delta t \approx 7$  [K]) where displacements  $u_{\max} < u_g$  one can use models  $a$ ,  $b$  and  $d$  from Fig. 4 (cases 1°-6°). However for  $u_{\max} > u_g$  (high temperature increase) the model from Fig. 4e is suitable.
4. Equally as in the case of  $\Delta N_{ii}$ , the effect of force  $\Delta N_{t,i+1}$  on the state of displacements and longitudinal forces in  $a_{i+1}$  segment of the CWR track (see Fig. 2) can be examined, assuming - in turn - for  $\Delta N_{t,i+1}$  the orientation of  $x$  axis of the local co-ordinates in the right-hand direction, according to the direction and orientation of this force.
5. For large values of  $\Delta t$ , e.g.  $\Delta t = 45$  [K], which are accompanied by high values of compressive forces in the rails, the CWR track is subjected to large longitudinal displacements, larger than  $u_g$ , taking place above all in the

breathing ends. For the analysis of such displacements of railway track models from Figs. 4a, b or c are suitable [2,3,4].

## REFERENCES:

1. Bałuch H.: Researches trends of jointless track at present operation requirements (in Polish). Materiały sympozjum „Budowa i utrzymanie toru bezстыkowego”, Zakopane 1996,
2. Bednarek Wł.: Stability analysis of jointless track in service in conditions of loss of contact with ballast (in Polish). PhD Thesis, Poznań 2002,
3. Bednarek Wł.: Loss of contact analysis in jointless track on ballast due to influence of non-axial horizontal subsoil reaction transfer. Archives of Civil Engineering, L. 3, 2004,
4. Bednarek Wł.: Practicability of longitudinal resistance models for effect analysis of local temperature change on axial displacement state in CWR track. 13<sup>th</sup> International Conference on Modernisation of Railway tracks, Slovakia, Žilina 2003,
5. Bednarek Wł.: Influence of selected models of ballast longitudinal resistance on confined length and breathing ends in continuous welded rail track (in Polish). Archiwum Instytutu Inżynierii Lądowej 3/2007 (materiały XIV Konferencji Naukowo-Technicznej „Drogi Kolejowe 2007”), Poznań-Rosnówko 2007,
6. Czyczuła Wł., Towpik K.: Estimation criterion of track structure due to permanent rails longitudinal displacements (in Polish). IX Krajowa Konferencja Naukowo-Techniczna „Drogi Kolejowe”, Kraków 1997,
7. Czyczuła Wł., Towpik K.: Modelling and identification problems of jointless track models (in Polish). Problemy kolejnictwa, zeszyt 128, Warszawa 1998,
8. Dieterman H. A., Van M. A., Van Damm A. J. P., Esveld C.: Longitudinal forces in railroad structures. Rail Engineering International, nr 1, 1990,
9. Esveld C.: Modern railway track, Second Edition, Delft 2001,
10. Huber M. T.: Works. Railway problems (in Polish). Vol. III, Part VIII (in Polish). PWN, Warsaw 1957,
11. Łoś M.: Influence of temperature on the behaviour of railway track (in Polish). Wydawnictwa Komunikacji i Łączności, Warsaw 1974,
12. PKP (Polish State Railways): Id-1 (D1). Technical conditions of track structure maintenance on railway lines (in Polish), Warsaw 2005,
13. Smekal A.: Transition structures of railway bridges. Materiały WCRR, Florencja 1997,
14. Szumierz W.: Statics of linear structures subjected to the action of horizontal forces due to creep of mining subsoil (in Polish). GIG (Central Institute of Mining), Katowice, 1980,
15. Szumierz W., J. Stefanek: Model of bridge interaction with a continuous welded rail track subjected to temperature changes. (in Polish). Drogi i mosty, nr 2, 2004,
16. Van M. A, Stability of continuous welded rail track. Delft 1995.